Author/s:
Betrie, AH;Abdul-Ridha, A;Hartono, H;Chalmers, DK;Wright, CE;Scott, DJ;Angus, JA;Ayton, S

Title:
The 8-hydroxyquinoline derivative, clioquinol, is an alpha-1 adrenoceptor antagonist

Date:
2024-04-01

Citation:
Betrie, A. H., Abdul-Ridha, A., Hartono, H., Chalmers, D. K., Wright, C. E., Scott, D. J., Angus, J. A. & Ayton, S. (2024). The 8-hydroxyquinoline derivative, clioquinol, is an alpha-1 adrenoceptor antagonist. Biochemical Pharmacology, 222, https://doi.org/10.1016/j.bcp.2024.116092.

Persistent Link:
https://hdl.handle.net/11343/344734

The 8-hydroxyquinoline derivative, clioquinol, is an alpha-1 adrenoceptor antagonist

Authors: Ashenafi H. Betrie[1,2,#], Alaa Abdul-Ridha[3,#], Herodion Hartono[4], David K. Chalmers[4], Christine E. Wright[5], Daniel J Scott[3], James A. Angus[5,] Scott Ayton[1*]

Affiliations:

[1]Translational Neurodegeneration Laboratory, Florey Institute of Neuroscience and Mental Health, The University of Melbourne, Victoria, Australia

[2]Preclinical Critical Care Unit, Florey Institute of Neuroscience and Mental Health, The University of Melbourne, Victoria, Australia

[3]Drug Discovery Innovation Group, Florey Institute of Neuroscience and Mental Health, The University of Melbourne, Victoria, Australia

[4]Faculty of Pharmacy and Pharmaceutical Sciences, Monash Institute of Pharmaceutical Sciences, Monash University, Victoria, Australia

[5]Department of Biochemistry and Pharmacology, The University of Melbourne, Victoria, Australia

[#]These authors contributed equally

*Correspondence to:

Scott Ayton, Florey Institute of Neuroscience and Mental Health, The University of Melbourne, VIC 3052, Australia. Tel.: +61 3 9035 6559; Email: scott.ayton@florey.edu.au

Declaration of Interest: None

Abstract

Clioquinol (5-chloro-7-iodo-8-hydroxyquinoline) is an antimicrobial agent whose actions as a zinc or copper ionophore and an iron chelator resurrected interest in similar compounds for the treatment of fungal and bacterial infections, neurodegeneration and cancer. Recently, we reported zinc ionophores, including clioquinol, cause vasorelaxation in isolated arteries through mechanisms that involve sensory nerves, endothelium and vascular smooth muscle. Here, we report that clioquinol also uniquely acts as a competitive alpha-1 (α_1) adrenoceptor antagonist. We employed *ex vivo* functional vascular contraction and pharmacological techniques in rat isolated mesenteric arteries, receptor binding assays using stabilized solubilized α_1 receptor variants, or wild-type human α_1-adrenoceptors transfected in COS-7 cells (African green monkey kidney fibroblast-like cells), and molecular dynamics homology modelling based on the recently published α_{1A} adrenoceptor crystal structure. At higher concentrations, all ionophores including clioquinol cause a non-competitive antagonism of agonist-mediated contraction due to intracellular zinc delivery, as reported previously. However, at lower concentration ranges, clioquinol has an additional mechanism of competitively inhibiting α_1-adrenoceptors that contributes to decreasing vascular contractility. Molecular dynamic simulation showed that clioquinol binds stably to the orthosteric binding site (Asp106) of the receptor, confirming the structural basis for competitive α_1-adrenoceptor antagonism by clioquinol.

Keywords:

Clioquinol, alpha 1 adrenoceptor, vascular contractility, vasorelaxation, zinc ionophores, molecular dynamic simulation, pharmacology

Abbreviations

AVP – Arginine vasopressin

CHESS – Cellular High-throughput Encapsulation, Solubilization, and Screening

COS-7 – African green monkey kidney fibroblast-like cells

DMSO – dimethyl sulfoxide

E_{max} – maximum possible effect of an agonist

K_B – dissociation constant

KPSS – potassium physiologic salt solution (124 mM K^+ replacing Na^+)

MeOx – methoxamine

PBT2 – 5,7-dichloro-2[(dimethylamino)methyl]-8-hydroxyquinoline

pEC_{50} – negative logarithm of EC_{50} (the concentration resulting in 50% of maximal response)

PSS – physiologic salt solution

QAPB – BODIPY-FL-labelled-prazosin

TRPA-1 – Transient receptor potential Ankyrin 1 channel

U46619 – 9,11-dideoxy-9a,11a-methanoepoxy prostaglandin $F_{2\alpha}$

Zn(DTSM) – Zinc(II)3,4-hexanedione bis[N(4)-methylthiosemicarbazone

Graphical Abstract

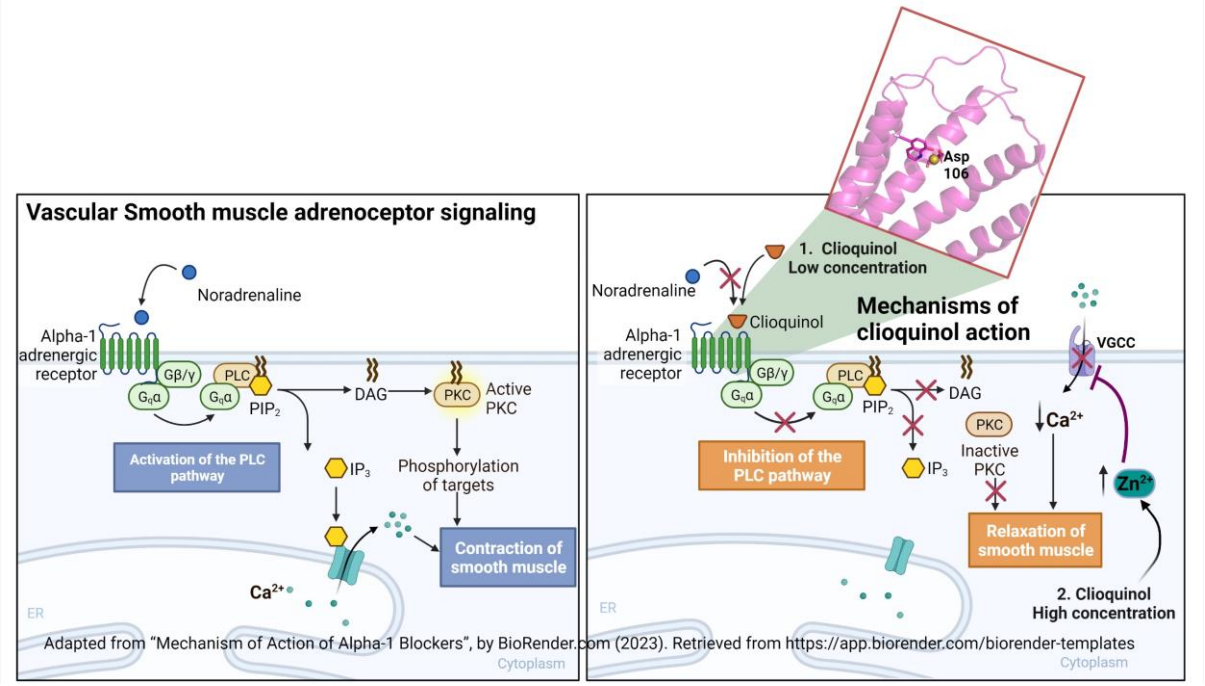

1. Introduction

Clioquinol (5-chloro-7-iodo-8-hydroxyquinoline) is an orally bioavailable, lipophilic, halogenated 8-hydroxyquinoline with antifungal, antiparasitic and potential anticancer activities. Clioquinol was used extensively in the mid-1900s as amebicide to treat diarrohea and indigestion but was eventually withdrawn from the market due to reports of subacute myelo-optic-neuropathy from Japan[1]. Clioquinol is currently available as a topical formulation for the treatment of skin and ear infections.

The ability of clioquinol to act as a zinc and copper ionophore and iron chelator[2] has revived the interest on this compound and its parent structure, 8-hydroxyquinoline, particularly in the treatment of neurodegeneration, cancer and infection. Clioquinol was effective in decreasing amyloid (Aβ) plaque in a transgenic animal model of Alzheimer's disease[3] which led to clinical trials of clioquinol [4] and other 8-hydroxyquinoline derivatives in patients[5-7] that showed conflicting results. Currently, there are increasing attempts to synthesize novel 8-hydroxyquinoline derivatives as potent antifungal agents [8], to break antibiotic resistance in bacterial infections [9], and to use clioquinol containing hybrid compounds for the treatment of neurodegeneration [10] and cancer [11]. Understanding the vascular effects of clioquinol will aid in designing both a selective agent for the different diseases where clioquinol or 8-hydroxyquinoline are used as parent compounds for medicinal chemistry.

We recently reported that zinc delivered to cells by ionophores such as clioquinol and pyrithione, drives vasorelaxation by mechanisms involving activation of transient receptor potential Ankyrin 1 (TRPA-1) in sensory nerves, increased synthesis of dilatory prostanoids from endothelium and inhibiting voltage-gated calcium channels in the vascular smooth muscle [12]. Here, we expand our investigations to assess if clioquinol acts as an α_1-adrenoceptor antagonist in addition to the mechanisms described previously. α_1-Adrenoceptors are seven

transmembrane domain G-protein coupled receptors for the endogenous catecholamines adrenaline and noradrenaline[13]. One of the most well- characterised actions of α_1-adrenoceptors is their role in vascular contraction where they are distributed across the medial and adventitial layers of the smooth muscle and endothelial cells[14]. All the three subtypes, α_{1A}, α_{1B} and α_{1D}-adrenoceptors are expressed in different vascular beds of mice, rats and humans [15-18],

To characterize if clioquinol acts as an α_1-adrenoceptor antagonist, we employed *ex vivo* functional vascular contraction and analytical pharmacological techniques in rat isolated mesenteric arteries, receptor binding assays using stabilized solubilized α_1 receptor variants engineered using Cellular High-throughput Encapsulation, Solubilization, and Screening (CHESS)[19] or the wild-type human α_1-adrenoceptors expressed in COS-7 cells, and molecular dynamics homology modelling based on the recently published α_{1A} crystal structure to probe the potential binding site[20, 21]. We find that clioquinol is a competitive antagonist of α_1-adrenoceptors at lower concentrations, which contributes to decreasing vascular contractility in addition to the previously described mechanisms of vasorelaxation at higher concentrations.

2. Materials and Methods

All animal experimental procedures were performed in accordance with the Australian code for the care and use of animals for scientific purposes (8th edition, 2013, National Health and Medical Research Council, Canberra) and were approved by the University of Melbourne Animal Ethics Committee (1212630, 1513798.1 and 1413363.1). Male Sprague Dawley rats (250–350 g) aged 8–12 weeks were obtained from the Biomedical Animal Facility, University of Melbourne, Victoria, Australia. All animals were group-housed in a climate-controlled facility (21 ± 1°C) with ambient humidity, a 12 h dark/light cycle and free access to food and

water. Rats were deeply anaesthetized by inhalation of 5% isoflurane (Baxter Healthcare, Australia) in O_2 and then were euthanized by rapid decapitation.

2.1. Functional *ex vivo* protocols in rat isolated mesenteric arteries

Rats were deeply anaesthetized by inhalation of 5% isoflurane (Baxter Healthcare, Australia) in O_2 and then euthanized by rapid decapitation. Approximately 10 cm of jejunum and its attached vascular fan was removed and pinned out on a Silastic-bottomed petri dish filled with ice-cold physiologic salt solution (PSS) with the following composition (mmol/L, mM): NaCl 119; KCl 4.69; $MgSO_4.7H_2O$ 1.17; KH_2PO_4 1.18; glucose 5.5; $NaHCO_3$ 25; $CaCl_2.6H_2O$ 2.5; EDTA 0.026 saturated with carbogen (O_2 95%; CO_2 5%) at pH 7.4.

Second or third order mesenteric arteries (250–350 μm internal diameter, i.d.) were isolated from the surrounding fat and connective tissue and ~2 mm length segments of arteries were mounted in separate myograph chambers (Model 610M and 620M; Danish Myo Technology, Denmark) containing PSS at 37°C for isometric force measurement as described previously[12, 22, 23]. Contractile responses were recorded with LabChart 7 and a PowerLab 4/30 A/D converter (AD Instruments Pty Ltd, Australia). To normalize the basal conditions, the vessels were passively stretched according to a normalization protocol and adjusted to a diameter setting of 90% of that determined for an equivalent transmural pressure of 100 mmHg. After allowing the tissues to equilibrate for 30 min, the arteries were exposed to a potassium depolarizing solution (124 mM K^+ replacing Na^+ in PSS; termed KPSS) and noradrenaline (10 μM) for 2 min. A second exposure to KPSS solution (only) was used to provide a reference contraction. Contraction responses were assessed by performing cumulative response curves to methoxamine (0.001–300 μM) in the absence (control) or presence of different concentration of clioquinol (3, 10, 30 μM), the classical zinc-complexed ionophore, zinc pyrithione, and ZnDTSM. Non-competitive antagonism due to the zinc-dependent vasorelaxant effects of

clioquinol[12] was assessed by using cumulative contraction response curves to endothelin-1 (0.1 – 300 nM), arginine vasopressin (0.01 – 10 nM) and U46619 (0.01 – 3 μM) in the absence or presence of different concentrations of clioquinol.

2.2. Functional α_1-adrenoceptor binding

To test the ability of clioquinol to bind α_1-adrenoceptors functionally, we measured the ability of clioquinol to protect α_1-adrenoceptors from inhibition by the irreversible antagonist benextramine[24, 25] in isolated arteries. A control methoxamine concentration-contraction curve was first completed in the absence of any treatment followed by wash out and incubation with clioquinol (10 μM) or an equivalent volume of the vehicle (DMSO) for 30 min. Then, both groups were incubated with benextramine (3 μM) for 5 min, while clioquinol or DMSO was still present. All the unbound treatments in the bathing solution were removed by 6 consecutive washes every 5 min, each containing 3 washes in quick succession and none of the agents were added back to the bathing solution. Due to the irreversible nature of benextramine inhibition, washing out will only remove the unbound free drug in the bath. The methoxamine concentration-contraction curve was then repeated.

α_1-Adrenoceptor competition binding assay in solubilized stable receptors

Binding of clioquinol was tested in detergent-stable, solubilized α_1-adrenoceptors previously described[19]. Briefly, 20 nmol of purified full-length biotinylated α_{1A}- or α_{1B}-adrenoceptor variant (mCherry attached to the C terminus) was resuspended in 10 ml of assay buffer (20 mM HEPES, pH 7.5, 100 mM NaCl, 0.05% DDM) and immobilized onto 200 μl of Dynabeads (Streptavidin T1) for 1 h at 4°C. 200 μl of the suspension-containing beads with immobilized receptor were aliquoted to a 96-Deep Well plate from which the beads were transferred to another 96-Deep Well plate containing 100 μl of ligand solution using a KingFisher Flex magnetic particle processor. For competition binding, immobilized receptors were incubated

with 100 µl of assay buffer containing 50 nM QAPB (quinazoline piperazine BODIPY) with ligands at various concentrations, for 2 h at 22°C. Immobilized receptors were subsequently washed with 200 µl of assay buffer and resuspended in 100 µl of assay buffer. Eighty µl of the final bead solution was transferred to a 96-well Greiner Bio-One nonbinding black plate. Fluorescence of bound QAPB was measured using a POLARstar OMEGA plate reader (BMG Labtech, Ortenburg, Germany) and normalized to mCherry fluorescence, which was detected simultaneously. Data represent the mean ±SEM of independent biological replicate experiments each performed in duplicate technical measurements.

2.3. Flow cytometry-based α_1-adrenoceptor binding assays

COS-7 cells were grown in DMEM with 10% FBS, 1% L-glutamine and 1% penicillin/ streptomycin. Cells were seeded at 300,000 cells/well on a 6-well–plate. The next day, cells were transiently transfected with 5 µg of receptor-IRES-mCherry DNA constructs per well, using Lipofectamine 2000 transfection reagent as per the manufacturer's instructions. After 48 h, the cells were resuspended in 2 mL of phenol red-free DMEM at 20°C and 50 µl of cell solution was added to each well of a clear v-bottom 96-well–plate. A further 50 µl of phenol red-free DMEM containing 12.5 nM QAPB with or without varying concentrations of competing ligands was added to relevant wells. The final concentrations of QAPB in all wells was 6.25 nM. Total binding was defined by the wells containing 6.25 nM QAPB only, whereas nonspecific binding was defined by wells containing 6.25 nM QAPB and 100 µM phentolamine. The cells were incubated with ligands for 1 h at 20°C on a shaking platform prior to detection of bound QAPB to mCherry-positive cells with flow cytometry using a Cytoflex LX cell analyser (Beckman Coulter). Flow cytometry data were then analysed in FlowJo to obtain QAPB mean fluorescence intensity (MFI) values from mCherry-positive cells. For each well, at least 5000 cells were used for data analysis.

2.4. Molecular dynamics homology modelling

All simulations were conducted using the CryoEM resolved structure of the human wildtype α_{1A}-adrenoceptor PDB ID: 7YM8 [21]. Only the receptor transmembrane structure was used in simulations while mini-Gs, nanobody 29, and oxymetazoline were excluded from simulations. Structures were pre-processed for missing side chains and protonation state using Protein Prep Wizard (part of Maestro Suite [26]) prior to docking and molecular dynamic simulations.

The docking of sodium dependent ligand was not supported by conventional docking methods, therefore manual docking using VMD [27] was used instead. Two binding poses were used based on different main contacts: Glu 180 of the extracellular loop 2 region, and Asp 106 of TM3 membrane in the orthosteric site. QAPB docking into receptor was by alignment to structure of α_{1B}-adrenoceptor bound to cyclazosin (PDB ID 7B6W [20]). Cyclazosin and QAPB share the core structure.

All simulations ran for 500ns on Gromacs 2021.5 [28]. All systems were in hexagonal tubes, consisting of the receptor, POPC bilayer and TIP3 water. Topology was built through a CHARMM-GUI server [29], with CHARMM36M force field parameters [30] for the receptor, water, ions, and lipids while CGENFF parameters [31] were used for organic ligands. Specific multi-site Ca^{2+} cation model was used on simulation 5 due to known improved accuracy [32]. Classical sphere was used for Zn^{2+} in simulation 6 which has been verified in other studies to be sufficient [33].

2.5. Inhibition of α_1-adrenoceptor signalling

To test the effects of clioquinol in α_1-adrenoceptor-mediated calcium signalling, calcium-dependent contraction was performed in tissues that were washed with a “calcium-free” buffer

followed by addition of PSS with methoxamine (10 μM) to cause receptor-dependent increase of cytosolic calcium. Increasing concentrations of calcium (0.01 – 10 mM) were then added to the bath to cause contraction (control first curve) followed by washout and incubation with a single concentration of test compounds (clioquinol or Zn(DTSM); second curve). Arteries were incubated with a single concentration of test compound for 15-20 min before the second concentration-contraction curve for calcium was completed.

2.6. Drugs

Drugs used in this study and their suppliers were: acetylcholine bromide (Sigma, St. Louis, MO, USA), arginine vasopressin (AusPep, Parkville, Victoria, Australia), benextramine tetrachloride (Sigma), BODIPY-FL-labelled-prazosin (QAPB) (Invitrogen, Australia), calcium chloride solution (Scharlab, Sentmenat, Spain), clioquinol (5-chloro-7-iodoquinolin-8-ol) (gift from Warner Babcock Institute (WBI), Massachusetts, USA), Dynabeads™ MyOne™ Streptavidin T1 beads (Invitrogen), endothelin-1 (AusPep), 8-hydroxyquinoline (gift from Dr Vijaya Kenche at the Florey Institute of Neuroscience and Mental Health, Australia), methoxamine hydrochloride (Sigma), [–]-noradrenaline bitartrate (Sigma), potassium chloride (Chem-Supply, South Australia, Australia), prazosin hydrochloride (Sigma), phentolamine hydrochloride (Sigma), U46619 (9,11-dideoxy-9a,11a-methanoepoxy prostaglandin $F_{2\alpha}$; Tocris Biosciences, Bristol, UK), Pytithione (Sigma), zinc chloride (Sigma), Zn(DTSM) (Zinc(II)3,4-hexanedione bis[N(4)-methylthiosemicarbazone]) (gifts from Warner Babcock Institute for Green Chemistry), zinc pyrithione (Sigma).

Stock solutions of 10 mM were made in DMSO (Ajax Finechem, Taren Point, NSW, Australia) of each of clioquinol, Zn(DTSM), 8-hydroxyquinoline, and U46619. Subsequent serial dilutions were made in ultrapure water (Milli-Q, Merck Millipore), except for clioquinol which was diluted to 1 mM in DMSO before being diluted in Milli-Q water. QAPB was made into in

methanol to 200 μM stock diluted in buffer to required concentrations when needed. All other drugs were prepared in Milli-Q water to 1 or 10 mM. Stock solutions were stored at -20°C except for pyrithione which was made daily to 20 mM in DMSO with addition of an equal volumes of 20 mM zinc chloride (Sigma) to a final concentration of 10 mM.

2.7. Data analyses

All data are expressed as mean ± SEM from n experiments each from separate animals, unless stated otherwise. Each sigmoidal concentration-response curve was fitted using Prism 7 (GraphPad Software, La Jolla, CA, USA). The pIC_{50} ± SEM values (the negative $\log_{10}$M of antagonist concentration that decreases the response to an agonist by 50%), E_{max} (maximum response of an agonist) were determined for each tissue and/or each concentration and averaged.

For binding assay in cells, the negative logarithm of the equilibrium dissociation constant for each ligand (pK_i) was obtained by fitting data to a one-site binding model, where the K_d of QAPB for each receptor (8 nM and 6 nM for α_{1A} or α_{1B}-adrenoceptors, respectively) and the concentration used in experiments (6.25 nM) was constrained[34].

Student's unpaired *t*-test was used to analyse the difference between two variables and one-way analysis of variance (1-way ANOVA) with Dunnett's or Tukey's post-test were used to compare means between three or more variables. The *p* values from the post-test are reported. Values of $p \leq 0.05$ were considered statistically significant.

2.7.1. Determination of functional antagonist potency

Antagonist potency in isolated small artery functional experiments was estimated by using the global regression method described by Lew and Angus[35] named the Clark plot. A non-linear regression plot of the agonist pEC_{50} values against different antagonist (B) concentrations (0,

3 and 10 μM) fitted by using equation (1) gives an estimate of the $p\mathrm{K_B}$ (-logK_B) and the confidence interval.

$$p\mathrm{EC_{50}} = \log[(B)^n + 10^{-p\mathrm{K_B}}] - \log c \qquad (1)$$

Where $p\mathrm{EC_{50}}$ denotes the negative logarithm of the $\mathrm{EC_{50}}$, (B) denotes antagonist concentration, log c (logarithm of the ratio of control $\mathrm{EC_{50}}$ to K_B) and $p\mathrm{K_B}$ denote fitting constants and n is a 'power departure' that is a measure of the molecularity of the antagonist-receptor interaction, equivalent to allowing the slope of a Schild plot to vary from unity[35, 36]. By allowing n to vary from unity the molecularity of the antagonist-receptor interaction can vary and using the goodness-of-fit of equation (1), the deviation of the concentration-effect curve spacing from the predictions of simple competitive antagonism can be tested.

3. Results

3.1. α_1-Adrenoceptor antagonism

We previously showed that zinc ionophores such as pyrithione and Zn(DTSM) (**Figure 1A**) relax arteries by mechanisms in sensory nerves, endothelium and vascular smooth muscle cells [12] . To test the competitive antagonism potential of clioquinol in α_1-adrenoceptors, we first used a direct analytical pharmacology approach. α_1-Adrenoceptor agonist-contraction curves were performed in rat mesenteric arteries using increasing concentrations of methoxamine in the presence or absence of clioquinol. Each artery segment was used for two methoxamine-contraction curves. There was no change in the potency (pEC$_{50}$ 5.80 ± 0.18 vs 5.92 ± 0.16, p>0.05) or the maximum α_1-adrenoceptor-mediated contractile responses (E_{max} 110 ± 3% KPSS vs 117 ± 3%, p>0.05, **Figure 1B**) between the first and second methoxamine curves with time.

Clioquinol caused a significant rightward shift of the methoxamine-induced contraction curve (**Figure 1C**). There was a 3.2-fold (pEC$_{50}$ 5.80 ± 0.18 vs 5.29 ± 0.08) and 10.3-fold (4.78 ± 0.12) rightward shift in the pEC$_{50}$ in the presence of 3 μM (p=0.019) and 10 μM clioquinol, respectively (p<0.0001 compared to control, 1-way ANOVA with Dunnett's post-test). The EC$_{50}$ for the 30 μM clioquinol was not calculated because of the near maximal inhibition of the contraction. The maximum response to methoxamine was decreased by the smaller concentration of clioquinol used (E_{max} 103 ± 3%, p=0.03 compared to control). In the presence of 10 μM clioquinol, the maximum methoxamine contraction at the highest concentration tested showed a significant decrease (E_{max} 85 ± 5% KPSS, p=0.0001 compared to control) and by 30 μM clioquinol, the contractile curve was completely inhibited (E_{max} 8 ± 7% KPSS, p=0.0001 compared to control, 1-way ANOVA with Dunnett's post-test; **Figure 1C**).

This rightward shift was not observed with zinc pyrithione (**Figure 1D**) or Zn(DTSM) (**Figure 1E**). Zinc pyrithione at 3 μM and 10 μM caused a decrease in the maximum contractile response to methoxamine (from E_{max} 117 ± 3% KPSS in control to 63 ±17 %, and 46 ± 12% and 20 ± 4% KPSS, respectively, p=0.0004, 1-way ANOVA with Dunnett's post-test). There was a rightward shift with the 3 μM (3.9-fold, pEC$_{50}$ 5.80 ± 0.19 vs 5.20 ± 0.18, n=7, p=0.04 and the 10 μM zinc pyrithione (2.8-fold, pEC$_{50}$ 5.80 ± 0.18 vs 5.35 ± 0.13, p>0.05 compared to control, 1-way ANOVA with Dunnett's post-test, **Figure 1D**). The lower concentration of Zn(DTSM) (3 μM) caused a decrease in the maximum contractile response to methoxamine (E_{max} 117 ± 4% KPSS in control vs 70 ±19% KPSS, p=0.027, 1-way ANOVA with Dunnett's post-test) and no change in sensitivity (pEC$_{50}$ 5.46 ± 0.11, n=4, p>0.05, unpaired t test). At higher concentrations, Zn(DTSM) almost completely blocked the contractile response by 94% and 83% compared to the control at 10 μM (E_{max} 7 ± 4% KPSS, p<0.0001) and 30 μM (E_{max} 20 ± 6% KPSS, p=0.0002, 1-way ANOVA with Dunnett's post-test), respectively (**Figure 1E**).

Competitive antagonism analysis using the Lew and Angus method

Clioquinol at lower concentrations, but not zinc pyrithione or Zn(DTSM) elicited a rightward displacement of the methoxamine concentration-contraction curves, suggesting a competitive nature of the antagonism of clioquinol. For simple competitive antagonism, the α_1-adrenoceptor antagonist dissociation constant (K_B) was determined by using the global regression method described by Lew and Angus[35].

The Lew and Angus[35] non-linear regression for clioquinol as a competitive antagonist gave an R^2 of 0.73 (17 d.f.) and n value of 1.17 ± 0.37. The n value showed a non-significant deviation from 1 suggesting a simple competitive antagonism fit. By constraining n to 1, the pK_B for clioquinol was 6.08 ± 0.17 (or K_B 0.832 μM). The Clark plot display (**Figure 2**) additionally showed that the average EC$_{50}$ values in the absence or presence of different

concentrations of clioquinol were placed within the ± 2 SEM of the non-linear regression global fit, further confirming the simple competitiveness of the antagonism. From the methoxamine concentration-contraction curves and Clark plot, clioquinol showed a competitive α_1-adrenoceptor antagonistic property up to 10 μM with an additional non-competitive vasorelaxant effect at the higher concentrations.

Protection of "irreversible" α_1-adrenoceptor antagonism

The rightward shifts of the methoxamine concentration-contraction curves induced by clioquinol reveals that lower concentrations of clioquinol (<10 μM) showed competitive antagonism of α_1-adrenoceptors. To further confirm this possibility, the ability of clioquinol to bind to α_1-adrenoceptors was tested by the two approaches: functional receptor protection and a competitive binding assay.

To test functional receptor protection, clioquinol was added to isolated mesenteric arteries to bind and protect α_1-adrenoceptors from subsequent irreversible inhibition by benextramine treatment. If clioquinol prevented the irreversible blockade of α_1-adrenoceptors by benextramine, this would give functional evidence of its ability to bind to the receptors. The control 1st methoxamine concentration-contraction curve gave a maximum contraction of 117 ± 5% KPSS with a $p\text{EC}_{50}$ value of 5.49 ± 0.09, (n=8, pooled). Incubation of a subset of these arteries with benextramine (3 μM) significantly decreased the maximum response seen to 54 ± 18% KPSS (a 52% decrease from the control curve, p=0.024, unpaired t test). The contraction $p\text{EC}_{50}$ value of methoxamine was also significantly right shifted by 7.1-fold to 4.53 ± 0.06 (p<0.0001, unpaired t test, **Figure 3A**).

Pre-treatment of the isolated mesenteric arteries with clioquinol (10 μM) for 30 min before addition of benextramine prevented the irreversible inhibition by benextramine. Clioquinol-treated small arteries contracted to 102 ± 5% KPSS with a $p\text{EC}_{50}$ of 5.09 ± 0.04, **Figure 3B**.

This represented a significant 88% increase in E_{max} (p=0.013) and 3.6-fold increase in sensitivity (p=0.003, 1-way ANOVA with Tukey's post-test, **Figure 3B**) compared to the benextramine alone-treated group. The clioquinol-treated group showed a modest 16% decrease in E_{max} (p=0.038) and a small but significant rightward shift in the pEC$_{50}$ (p=0.014, unpaired t test) compared to the control group.

Binding of clioquinol to human α_{1A} and α_{1B}-adrenoceptors

To confirm the functional antagonistic effects seen in rat isolated mesenteric arteries, a direct competitive binding assay was performed using detergent-stable, solubilized human α_{1A} and α_{1B}-adrenoceptors described in Yong *et al*. [19]. The binding was then repeated using wild-type human α_{1A} and α_{1B}-adrenoceptors expressed in COS-7 cells.

In solubilized, detergent-stable receptors, clioquinol and its parent compound 8-hydroxyquinoline showed a concentration-dependent competitive binding at the α_{1A}-adrenoceptors (pK$_I$ = 4.87 ± 0.30 and 4.49 ± 0.76, respectively, **Figure 4A**) and α_{1B}-adrenoceptors (pK$_I$ = 5.02 ± 0.24 and 6.01 ± 0.36, respectively, **Figure 4B**). Zinc pyrithione, on the other hand, failed to show binding at either receptor. The binding of clioquinol and 8-hydroxyquinoline elicited a 24 ± 8% and 13 ± 7% decrease in non-selective fluorescently labelled antagonist QAPB binding.

The binding profiles of clioquinol were also examined in a flow cytometry-based binding assay using 6.25 nM of the QAPB. Similar to the stabilised receptors, the equilibrium competitive binding studies in COS-7 cells transiently expressing WT α_{1A}- or α_{1B}-adrenoceptors revealed that clioquinol binds to these receptors with low affinity (K_i) (pK$_I$ = 3.75 ± 0.16 at α_{1A} and pK$_I$ = 3.48 ± 0.28 at α_{1B}-adrenoceptors) **(Figure 4C**). In this case, clioquinol was able to cause a full competition at the highest concentration tested.

Docking and molecular dynamics simulations of clioquinol binding

Docking and molecular dynamics simulations were performed to investigate the binding location of clioquinol to the α_{1A}-adrenoceptor, including the involvement of cation bridging interactions between the drug and receptor. Six simulations of 500 ns in total were run (**Table 1**). Simulations were run in water containing 150 mM NaCl. In an initial simulation of the apo receptor (**S1**), we observed that sodium ions contacted two acidic residues, Glu180 in the outer binding pocket and Asp106 which forms part of the orthosteric binding site (**Figure 5A**). Contacts were maintained for at least 200 ns (**Figure 6A**). In simulation S2, QAPB was docked by alignment with the crystal structure of cyclazosin in the α_{1B}-adrenoceptor (**Figure 5B**). QABP remained stable in this location for the full 500 ns of the simulation (**Figure 6B**). To create the starting geometry for simulations S3 and S4 (**Figures 5C** and **5D**), clioquinol was placed so that the drug nitrogen and oxygen atoms contacted sodium ions bound to residues Asp 106 and Glu 180 respectively and the drug also overlapped with the QABP binding site. The drug bound in the orthosteric binding site was stable throughout the whole simulation, while the bound conformation in outer pocket was unstable and the ligand left the pocket (**Figure 6C**). In simulations S5 and S6 the counterion was substituted by Ca^{2+} and Zn^{2+} at the orthosteric binding site (**Figure 5D and E**). In simulation S5, the Ca^{2+} ion was represented using a multi-site model [32]. In both cases, the bound ligand remained stable for the full 500 ns simulation (**Figure 6D**).

Inhibition of calcium signalling using a functional assay

To examine the effect of clioquinol in intracellular signalling, a single high concentration (10 μM) of the α_1-adrenoceptor agonist, methoxamine, was used to stimulate the opening of calcium channels in isolated small mesenteric arteries. A cumulative calcium-contraction curve

was then completed without (control 1st curve) or with different concentrations of clioquinol (second curves).

The sensitivity (pEC$_{50}$) or the maximum α_1-adrenoceptor-dependent calcium-induced contractile responses were not affected by time or vehicle (DMSO) (**Figure 7A, Table 2**). After establishing this, the effects of clioquinol in the α_1-adrenoceptor-dependent calcium-induced contractile responses were investigated. The control 1st curve had a maximum methoxamine-stimulated, calcium-induced contraction of 111 ± 4% KPSS with pEC$_{50}$ of 3.92 ± 0.03 (n=13, **Figure 7B**). Clioquinol showed a concentration-dependent effect in the α_1-adrenoceptor-dependent calcium-induced contraction. Incubation of arteries with 3 μM clioquinol caused a modest but significant 1.5-fold rightward shift in the pEC$_{50}$ to 3.73 ± 0.04 (p=0.007 compared to control, 1-way ANOVA with Dunnett's post-test; **Figure 7B, Table 2**) without affecting the maximum response (E_{max} 107 ± 4% KPSS, n=5). Increasing the clioquinol concentration to 10 μM induced a significant 2.7-fold decrease in the sensitivity of the isolated mesenteric artery to calcium (pEC$_{50}$ 3.49 ± 0.05, p=0.0001, 1-way ANOVA with Dunnett's post-test) without affecting the E_{max} (101 ± 6% KPSS, n=5, p>0.05; **Figure 7B, Table 2**). A further increase in the concentration of clioquinol to 30 μM abolished the calcium-induced contraction (E_{max} 2 ± 1% KPSS, n=4, p=0.0001, 1-way ANOVA with Dunnett's post-test).

The zinc ionophore, Zn(DTSM) showed a rightward shift of the calcium-dependent contraction from pEC$_{50}$ of 3.87 ± 0.04, to 3.57 ± 0.07 at 3 μM (p=0.002) and 3.20 ± 0.07 at 10 μM (p=0.0001, 1-way ANOVA with Dunnett's post-test) but had a significantly lowered maximum contraction **(Figure 7C, Table 2**). Thus, clioquinol not only shows competitive antagonism at the receptor level, but also intracellularly changes the sensitivity to calcium signalling after agonism by the α_1-adrenoceptor agonist, methoxamine.

Non-competitive antagonism of endothelin, vasopressin and thromboxane–mediated vascular contraction.

To assess if the effects of clioquinol on α-adrenoceptor-mediated contraction were also seen with other contractile receptors, agonists endothelin-1 (0.1 – 300 nM), arginine vasopressin (0.01 – 10 nM) and U46619 (0.01 – 3 μM) were tested in the absence and presence of clioquinol.

Endothelin-1 induced concentration-dependent contraction (E_{max} 114 ± 4% KPSS, n=5) with a pEC_{50} of 7.55 ± 0.16 in rat mesenteric arteries (**Figure 8A**). Clioquinol pre-treatment (3 μM) did not significantly affect the sensitivity (pEC_{50} 7.69 ± 0.03, n=4) or E_{max} (107 ± 6% KPSS). Increased concentrations of clioquinol to 10 μM, 20 μM or 30 μM, on the contrary, elicited concentration-dependent decreases in the E_{max} to 84 ± 9% (n=6, p=0.009), 57 ± 4% (n=5, p=0.0001) and 35 ± 7% KPSS (n=4, p=0.0001, 1-way ANOVA with Dunnett's post-test, **Figure 8A**), respectively. None of the concentrations of clioquinol affected the sensitivity of the small mesenteric arteries to endothelin-1.

Arginine vasopressin (AVP) caused a maximum contraction of 103 ± 5% KPSS with a pEC_{50} of 9.08 ± 0.18 (n=6, **Figure 8B**). Clioquinol (10 μM) pre-treatment caused a significant 22% decrease in the E_{max} to 81 ± 7% KPSS (n=5, p=0.03, 1-way ANOVA with Dunnett's post-test), without a statistically significant shift in the AVP pEC_{50} (8.78 ± 0.09). A further increase in the concentration of clioquinol to 20 μM decreased the E_{max} to 17 ±5% KPSS (n=6, p=0.0001), while 30 μM almost completely abolished the AVP-induced contraction (E_{max} 6 ± 2%KPSS, p=0.0001, 1-way ANOVA with Dunnett's post-test, **Figure 8B**). The pEC_{50} of AVP in the presence of 20 μM and 30 μM clioquinol was not calculated due to the small effects. Addition of a maximum equivalent volume of vehicle (DMSO) did not significantly affect either the E_{max} or pEC_{50} compared to the control (data not shown).

The thromboxane mimetic, U46619, caused a maximum contraction of 118 ± 4% KPSS with a $p\mathrm{EC}_{50}$ of 6.62 ± 0.06 (n=6, **Figure 8C**). Incubation with 3 and 10 μM clioquinol did not significantly affect the E_{max} or sensitivity. Incubation with 20 and 30 μM on the other hand caused a significant 60% (E_{max} 47 ± 14% KPSS) and 93% (E_{max} 8 ± 3% KPSS) inhibition of the E_{max} compared to the control (p=0.0001, 1-way ANOVA with Dunnett's post-test, **Figure 8C**), without a change in the $p\mathrm{EC}_{50}$. Although there was no significant change in the sensitivity of the small arteries to U46619, there was a noticeable variation between individual $p\mathrm{EC}_{50}$ values in the presence of clioquinol as evidenced by the large standard error. An equivalent maximum volume of the vehicle (DMSO) caused a moderate 2.4-fold rightward shift of the U46619 $p\mathrm{EC}_{50}$ (7.01 ± 0.16, p=0.02, unpaired t test), without significantly affecting the E_{max} (127 ± 0.9, n=4, p=0.09, unpaired t test, data not shown).

4. Discussion

We previously reported that ionophores such as clioquinol, zinc pyrithione and Zn(DTSM) can transport zinc intracellularly in the vasculature, and hence elicit vasorelaxation [12]. The mechanisms we identified involved the activation of TRPA1 channels in sensory nerves that then release calcitonin gene-related peptide, the synthesis of dilatory prostacyclin from endothelial cells and the inhibition of voltage-gated calcium channels in vascular smooth muscle cells. Owing to the differences in chemical structure and the multitude of effects that zinc has, the presence of additional mechanisms for the vasorelaxant action of zinc ionophores was a possibility. Here, we observed an additional mechanism of action by clioquinol in antagonising α_1-adrenoceptor-mediated contraction.

Lower concentrations (up to 10 μM) of clioquinol had a competitive α_1-adrenoceptor antagonistic property with a pK_B of 6.08 ± 0.17 in rat isolated mesenteric arteries. Higher concentrations (above 10 μM), however showed non-competitive, functional antagonism possibly due to the previously described mechanisms that are mediated by zinc (the activation of TRPA1 channels in sensory nerves, the synthesis of dilatory prostacyclin from endothelial cells and the inhibition of voltage-gated calcium channels in vascular smooth muscle cells [12]). The other zinc ionophores, zinc pyrithione and Zn(DTSM) only showed non-competitive, functional antagonism. To our knowledge, this is the first time the α_1-adrenoceptor antagonist effect of clioquinol has been reported. In accord to this finding, we previously reported that clioquinol (10 μM) also inhibited electrical nerve stimulation-dependent contraction that is elicited by the release of noradrenaline from perivascular sympathetic nerves of rat mesenteric arteries [12].

Although we could not find similar articles reporting the role of clioquinol on α_1, α_2 or β-adrenoceptor function, the parent compound 8-hydroxyquinoline has previously been shown

to inhibit the cathecholamine metabolising enzyme cathecol-o-methyl transferase [37] and noradrenaline uptake in rabbit aorta [38]. The contractile response to electrically-stimulated neurogenic contractile response (estimated EC_{50} ~100 μM) as well as to exogenous noradrenaline and serotonin in rabbit isolated pulmonary arteries were blocked by 8-hydroxyquinoline [38]. The authors argued that these inhibitory effects may be due to the ability of 8-hydroxyquinoline to chelate trace metals.

The simple competitive nature of the antagonism was confirmed by using the global regression method described by Lew and Angus [35] which in this study has a clear, definite advantage over the classical Schild analysis. Schild analysis overemphasizes the control concentration-response curve which affects the accuracy of every dose ratio. Besides, the use of a single methoxamine concentration-response curve in the absence or presence of the antagonist clioquinol doesn't allow the historical approach by Arunlakshana and Schild [36] where a single tissue is used repetitively to construct the agonist concentration-response curves in the absence (control) and presence of different concentrations of the antagonist and calculates the rightward shift in the EC_{50} concentration ratio from the control curve. The vasorelaxant effect of clioquinol takes a considerable amount of time to washout making it practically challenging to construct repetitive concentration-response curves with different concentrations of clioquinol.

Based on the Clark plot, simple competitive antagonism can be tested by two methods. The first is to check if *n* (from Eq (1) is not significantly different from 1 (e.g. if the 95% confidence interval for n contains 1); if so, it suggests that the spacings of the agonist concentration-response curves in the absence and presence of the antagonist are consistent with a simple competitive interaction. In the functional receptor binding experiment, the parameter *n* was not significantly different from 1. The *n* in this circumstance is constrained to unity, and the resulting *p*K value is then equivalent to the pK_B. The second is to use Clark plot, the display of

the actual mean pEC_{50} values against the antagonist concentration $-\log(B+K_B)$ [39]. The error bars in the Clark plot are ± 2 standard error of the differences between the observed and predicted pEC_{50} values from fitted Eq (1), an estimate of the confidence interval around the line. If the point showing the mean observed pEC_{50} values at a level of $-\log(B+K_B)$ falls outside the error bar, this indicates a departure from a simple competitive interaction. And based on these two methods, clioquinol fulfils a simple competitive antagonistic activity up to 10 μM but has an additional non-competitive antagonistic effect beyond this concentration. It is worth noting that the maximum methoxamine contraction was significantly lower than in the control. As such this may be due to functional antagonistic mechanisms reported previously that start to come to play at this concentration. However, the fact that the error bars in the Clark plot fall within 2 standard error of the difference between the observed and predicted pEC_{50} fulfils the criterion for simple competitive antagonism.

A non-competitive antagonist can cause a similar rightward shift in the methoxamine concentration-response curve due to the presence of α_1-adrenoceptor reserve. The maximum contractile effects in arteries due to α_1-adrenoceptors do not need maximal receptor occupancy [40]. Presence of a reserve pool of α_1-adrenoceptors also known as "spare receptors" ensures maximum effects are seen with less than maximal receptor occupancy [41]. Due to these spare receptors, an effective non-competitive vasodilator agent that does not employ α_1-adrenoceptors may still show a rightward shift without affecting the E_{max} until the receptor reserve is entirely occupied by the α_1-adrenoceptor agonist methoxamine [42]. In this study, two separate types of experiments provided evidence for the ability of clioquinol to bind to α_1-adrenoceptors. The first, a functional study, (**Figure 3**) showed that pre-treatment of arteries with clioquinol (10 μM) for 30 min prevented the irreversible inhibition of α_1-adrenoceptors by subsequent incubation with benextramine. Benextramine (3 μM) alone shifted the methoxamine concentration-effect curve by about 7-fold to the right and decreased the

maximum response by 54% consistent with the property of a non-competitive inhibitor in the presence of "spare receptors". Arteries pre-treated with clioquinol showed a significant prevention of the rightward shift in the EC_{50} as well as in the maximum response, suggesting the direct binding of clioquinol to α_1-adrenoceptors. The inhibition of α_1-adrenoceptor-mediated contraction by the other zinc ionophores, zinc pyrithione and Zn(DTSM) followed a similar pattern to benextramine where there was a small shift in the response to the right, possibly due to the functional antagonism eliciting the use of spare receptors, followed by depression of the maximum response consistent with non-competitive antagonism for a GPCR with "spare receptors".

In mouse isolated arteries, functional vasoconstrictor responses in isolated arteries highlighted the contribution of α_{1A}-adrenoceptors in mesenteric and caudal arteries and that of α_{1D} in carotid arteries and the aorta, but there was also a minor role for α_{1B}-adrenoceptors in vasoconstriction[43]. In rat mesenteric arteries, pharmacological antagonists suggests only a small contribution of α_{1A}-adrenoceptors to contraction, with prominent roles for α_{1L} functional subtype receptor [15-18], α_{1D} [17] and α_{1B}-adrenoceptors [17, 18]. The crystal structures of α_{1A} and α_{1B}-adrenoceptors were recently solved [20, 21]. Therefore, to assess the binding of clioquinol to α_1-adrenoceptors, we used both detergent-stable, solubilized human α_{1A} and α_{1B}-adrenoceptors as well as wild-type receptors transfected and expressed in COS-7 cells. α_{1D}-adrenoceptors are known to be poorly expressed at the cell-surface [44] and we could not detect any QAPB binding (data not shown). .

In detergent-stable and solubilized human α_1-adrenoceptors, both the parent compound 8-hydroxyquinoline and clioquinol showed a weak, partial competitive antagonism at an affinity close to the rat receptors in isolated mesenteric arteries. The binding affinity was more potent in stabilized α_{1B}- than α_{1A}-adrenoceptors. Clioquinol also showed full competitive antagonism in the wild type α_1-adrenoceptors expressed in COS-7 cells albeit at a much lower affinity

compared to the rat receptors or the stabilized human α_1-adrenoceptors. This suggests differences in binding affinity due to species (rat vs human) and type of tissue/cells used (isolated mesenteric arteries which can have different density of the α_1-adrenoceptor subtypes, spare receptors and endogenous signalling mechanism compared to cells solely expressing one receptor subtype). In this binding assay, another classical zinc ionophore, zinc pyrithione, failed to show any competitive binding suggesting that the zinc-bound ionophore, which can easily be internalized, is unlikely to contribute to the receptor binding on the extracellular orthosteric binding pocket of the α_1-adrenoceptors.

We previously reported that one of the vasorelaxation mechanisms for clioquinol (in the absence of added exogenous zinc) is non-competitive inhibition of voltage-operated calcium channel-dependent responses [12]. This alludes to the fact that at lower concentrations, the apo-clioquinol (without zinc) acts as a competitive α_1-adrenoceptor antagonist by binding to the orthosteric binding pocket of the receptors at cell surface, as confirmed by the molecular dynamics data. This is also further supported by the fact that similar concentrations cause a competitive shift in the cytoplasmic calcium-dependent contractions.

Molecular dynamics simulation S3 demonstrated that clioquinol binding is stable in the orthosteric pocket. The binding of ligands to GPCRs with cation bridges has been known to happen with the conserved aspartic acid, such as in melanocortin receptor [45]. Simulations S5 and S6 showed that both Ca^{2+} and Zn^{2+} as the cation bridge will result in a similarly stable binding conformation. All together molecular dynamic simulations demonstrated that clioquinol is likely an orthosteric binder to the α_{1A}-adrenoceptor with a cation bridged interaction to the conserved aspartic acid residue.

However, we cannot exclude the potential of clioquinol to complex with trace amounts of zinc present in the extracellular solution or redistribute zinc in organelles such as mitochondria,

Golgi and lysosomes [46]. The ability of clioquinol to redistribute zinc has been shown in neurodegeneration [47, 48]. In such instances, one would expect the clioquinol to be internalized rather than binding to an extracellular binding pocket of the α_1-adrenoceptor. Boedtkjer *et. al.* [49] reported that 30 min incubation with 10 μM zinc chloride extracellularly causes a rightward shift in the noradrenaline contraction curve in rat isolated mesenteric arteries suggesting that zinc by itself may have ability to bind and antagonize α_1-adrenoceptors. Further, an allosteric binding site for zinc on β_2-adrenoceptors [50] and inhibition of β-adrenoceptor stimulation of ventricular cardiomyocytes by intracellular zinc were previously reported [51]. These studies and our data suggest that both zinc and clioquinol can have direct inhibitory effects on adrenoceptors on plasma-membrane independently of each other or coordinate to redistribute zinc for a non-competitive antagonism. Our data demonstrate that in addition to the previously reported non-competitive antagonism mechanism, clioquinol showed a consistent non-competitive inhibitory effect of other agonists such as endothelin 1, AVP and U46619 at higher concentrations (>10 μM; **Figure 8**) without affecting sensitivity to the responses. This further implies the presence of another common downstream intracellular mechanism responsible for the vasorelaxant effects of clioquinol, in addition to the competitive α_1-adrenoceptor antagonism. Collectively, our study shows that clioquinol can bind to α_1-adrenoceptors at the orthosteric binding site. We show that clioquinol is a competitive antagonist at lower concentrations as shown by rat isolated mesenteric artery vasocontractile responses to methoxamine, ability to protect α_1-adrenoceptors from irreversible binding by benextramine, shift in the calcium-dependent signalling, functional binding in human α_{1A}- and α_{1B}-adrenoceptors expressed in cells as well as docking and molecular dynamic simulations. These results may provide an insight into one of the common side effects of clioquinol use as antifungal agent – rapid hair growth in the areas of local application [52]. Hair growth is a common side effect of vasodilator use that was explored as a therapeutic for hair loss [53].

These results also have implication to predicting the potential contribution of vasorelaxation to the mechanism of action or side effect profile of newer drug derivatives that use the parent compound 8-hydroxyquinoline or clioquinol for the treatment of fungal or bacterial infections, cancer and Alzheimer's disease. Systemic use of these compounds may be a potential cause of drug interaction or enhanced efficacy of other treatments used for cardiovascular diseases such as hypertension. Further, these results may be useful for understanding the vascular mechanisms of clioquinol action, and future drug development that may use it as the parent compound for medicinal chemistry to identify vasodilator agents that target more than one mechanisms of action.

Acknowledgements

We thank Ms. Linda Cornthwaite-Duncan for assistance with the myography experiments. This work was funded by the Australian National Health and Medical Research Council. The Florey Institute of Neuroscience and Mental Health acknowledges support from the Victorian Government, in particular, funding from the Operational Infrastructure Support Grant.

5. References:

[1] T.W. Meade, Subacute myelo-optic neuropathy and clioquinol. An epidemiological case-history for diagnosis, Br. J. Prev. Soc. Med. 29(3) (1975) 157-69.

[2] E. Ferrada, V. Arancibia, B. Loeb, E. Norambuena, C. Olea-Azar, J.P. Huidobro-Toro, Stoichiometry and conditional stability constants of Cu(II) or Zn(II) clioquinol complexes; implications for Alzheimer's and Huntington's disease therapy, Neurotoxicology 28(3) (2007) 445-449.

[3] R.A. Cherny, C.S. Atwood, M.E. Xilinas, D.N. Gray, W.D. Jones, C.A. McLean, K.J. Barnham, I. Volitakis, F.W. Fraser, Y. Kim, X. Huang, L.E. Goldstein, R.D. Moir, J.T. Lim, K. Beyreuther, H. Zheng, R.E. Tanzi, C.L. Masters, A.I. Bush, Treatment with a copper-zinc chelator markedly and rapidly inhibits beta-amyloid accumulation in Alzheimer's disease transgenic mice, Neuron 30(3) (2001) 665-76.

[4] C.W. Ritchie, A.I. Bush, A. Mackinnon, S. Macfarlane, M. Mastwyk, L. MacGregor, L. Kiers, R. Cherny, Q.X. Li, A. Tammer, D. Carrington, C. Mavros, I. Volitakis, M. Xilinas, D. Ames, S. Davis, K. Beyreuther, R.E. Tanzi, C.L. Masters, Metal-protein attenuation with iodochlorhydroxyquin (clioquinol) targeting Aβ amyloid deposition and toxicity in Alzheimer disease: a pilot phase 2 clinical trial, Arch. Neurol. 60(12) (2003) 1685-91.

[5] L. Lannfelt, K. Blennow, H. Zetterberg, S. Batsman, D. Ames, J. Harrison, C.L. Masters, S. Targum, A.I. Bush, R. Murdoch, J. Wilson, C.W. Ritchie, P.E.s. group, Safety, efficacy, and biomarker findings of PBT2 in targeting Aβ as a modifying therapy for Alzheimer's disease: a phase IIa, double-blind, randomised, placebo-controlled trial, Lancet Neurol. 7(9) (2008) 779-86.

[6] N.G. Faux, C.W. Ritchie, A. Gunn, A. Rembach, A. Tsatsanis, J. Bedo, J. Harrison, L. Lannfelt, K. Blennow, H. Zetterberg, M. Ingelsson, C.L. Masters, R.E. Tanzi, J.L. Cummings, C.M. Herd, A.I. Bush, PBT2 rapidly improves cognition in Alzheimer's Disease: additional phase II analyses, J. Alzheimers Dis. 20(2) (2010) 509-16.

[7] P.J. Crouch, M.S. Savva, L.W. Hung, P.S. Donnelly, A.I. Mot, S.J. Parker, M.A. Greenough, I. Volitakis, P.A. Adlard, R.A. Cherny, C.L. Masters, A.I. Bush, K.J. Barnham, A.R. White, The Alzheimer's therapeutic PBT2 promotes amyloid-beta degradation and GSK3 phosphorylation via a metal chaperone activity, J. Neurochem. 119(1) (2011) 220-30.

[8] L. Li, H. Wu, J. Wang, Z. Ji, T. Fang, H. Lu, L. Yan, F. Shen, D. Zhang, Y. Jiang, T. Ni, Discovery of Novel 8-Hydroxyquinoline Derivatives with Potent In Vitro and In Vivo Antifungal Activity, J. Med. Chem. (2023).

[9] E.B. Brazel, A. Tan, S.L. Neville, A.R. Iverson, S.R. Udagedara, B.A. Cunningham, M. Sikanyika, D.M.P. De Oliveira, B. Keller, L. Bohlmann, I.M. El-Deeb, K. Ganio, B.A. Eijkelkamp, A.G. McEwan, M. von Itzstein, M.J. Maher, M.J. Walker, J.W. Rosch, C.A. McDevitt, Dysregulation of Streptococcus pneumoniae zinc homeostasis breaks ampicillin resistance in a pneumonia infection model, Cell Rep 38(2) (2022) 110202.

[10] X. Li, T. Li, P. Zhang, X. Li, L. Lu, Y. Sun, B. Zhang, S. Allen, L. White, J. Phillips, Z. Zhu, H. Yao, J. Xu, Discovery of novel hybrids containing clioquinol-1-benzyl-1,2,3,6-tetrahydropyridine as multi-target-directed ligands (MTDLs) against Alzheimer's disease, Eur. J. Med. Chem. 244 (2022) 114841.

[11] M. Zhang, L. Li, S. Li, Z. Liu, N. Zhang, B. Sun, Z. Wang, D. Jia, M. Liu, Q. Wang, Development of Clioquinol Platinum(IV) Conjugates as Autophagy-Targeted Antimetastatic Agents, J. Med. Chem. 66(5) (2023) 3393-3410.

[12] A.H. Betrie, J.A. Brock, O.F. Harraz, A.I. Bush, G.W. He, M.T. Nelson, J.A. Angus, C.E. Wright, S. Ayton, Zinc drives vasorelaxation by acting in sensory nerves, endothelium and smooth muscle, Nat Commun 12(1) (2021) 3296.

[13] J. Akinaga, J.A. García-Sáinz, S.P. A, Updates in the function and regulation of α(1) -adrenoceptors, Br. J. Pharmacol. 176(14) (2019) 2343-2357.

[14] J.C. McGrath, Localization of α-adrenoceptors: JR Vane Medal Lecture, Br. J. Pharmacol. 172(5) (2015) 1179-94.

[15] W.B. Stam, P.H. Van der Graaf, P.R. Saxena, Analysis of alpha 1L-adrenoceptor pharmacology in rat small mesenteric artery, Br. J. Pharmacol. 127(3) (1999) 661-70.

[16] N.A. Flavahan, P.M. Vanhoutte, α1-Adrenoceptor subclassification in vascular smooth muscle, Trends Pharmacol. Sci. 7 (1986) 347-349.

[17] L.E. Arévalo-León, I.A. Gallardo-Ortíz, H. Urquiza-Marín, R. Villalobos-Molina, Evidence for the role of alpha1D- and alpha1A-adrenoceptors in contraction of the rat mesenteric artery, Vascul. Pharmacol. 40(2) (2003) 91-6.

[18] M.B. Hussain, I. Marshall, Alpha(1)-adrenoceptor subtypes mediating contractions of the rat mesenteric artery, Eur. J. Pharmacol. 395(1) (2000) 69-76.

[19] K.J. Yong, T.M. Vaid, P.J. Shilling, F.J. Wu, L.M. Williams, M. Deluigi, A. Plückthun, R.A.D. Bathgate, P.R. Gooley, D.J. Scott, Determinants of Ligand Subtype-Selectivity at α(1A)-Adrenoceptor Revealed Using Saturation Transfer Difference (STD) NMR, ACS Chem. Biol. 13(4) (2018) 1090-1102.

[20] M. Deluigi, L. Morstein, M. Schuster, C. Klenk, L. Merklinger, R.R. Cridge, L.A. de Zhang, A. Klipp, S. Vacca, T.M. Vaid, P.R.E. Mittl, P. Egloff, S.A. Eberle, O. Zerbe, D.K. Chalmers, D.J. Scott, A. Pluckthun, Crystal structure of the alpha1B-adrenergic receptor reveals molecular determinants of selective ligand recognition, Nat Commun 13(1) (2022) 382.

[21] Y. Toyoda, A. Zhu, F. Kong, S. Shan, J. Zhao, N. Wang, X. Sun, L. Zhang, C. Yan, B.K. Kobilka, X. Liu, Structural basis of α(1A)-adrenergic receptor activation and recognition by an extracellular nanobody, Nat Commun 14(1) (2023) 3655.

[22] J.A. Angus, C.E. Wright, Techniques to study the pharmacodynamics of isolated large and small blood vessels, J. Pharmacol. Toxicol. Methods 44(2) (2000) 395-407.

[23] A.H. Betrie, S. Ayton, A.I. Bush, J.A. Angus, P. Lei, C.E. Wright, Evidence of a cardiovascular function for microtubule-associated protein tau, J. Alzheimers Dis. 56(2) (2017) 849-860.

[24] M.J. Lew, J.A. Angus, Reversible inhibition of neuronal uptake by benextramine, an irreversible presynaptic alpha-adrenoceptor antagonist, Eur J Pharmacol 98(1) (1984) 27-34.

[25] C. Melchiorre, M.S. Yong, B.G. Benfey, B. Belleau, Molecular properties of the adrenergic .alpha. receptor. 2. Optimum covalent inhibition by two different prototypes of polyamine disulfides, J. Med. Chem. 21(11) (1978) 1126-1132.

[26] S. Maestro, LLC. Schrödinger release 2021-1, 2021.

[27] W. Humphrey, A. Dalke, K. Schulten, VMD: visual molecular dynamics, J. Mol. Graph. 14(1) (1996) 33-8, 27-8.

[28] M.J. Abraham, T. Murtola, R. Schulz, S. Páll, J.C. Smith, B. Hess, E. Lindahl, GROMACS: High performance molecular simulations through multi-level parallelism from laptops to supercomputers, SoftwareX 1-2 (2015) 19-25.

[29] S. Jo, X. Cheng, J. Lee, S. Kim, S.J. Park, D.S. Patel, A.H. Beaven, K.I. Lee, H. Rui, S. Park, H.S. Lee, B. Roux, A.D. MacKerell, Jr., J.B. Klauda, Y. Qi, W. Im, CHARMM-GUI 10 years for biomolecular modeling and simulation, J. Comput. Chem. 38(15) (2017) 1114-1124.

[30] J. Huang, S. Rauscher, G. Nawrocki, T. Ran, M. Feig, B.L. de Groot, H. Grubmüller, A.D. MacKerell, CHARMM36m: an improved force field for folded and intrinsically disordered proteins, Nat. Methods 14(1) (2017) 71-73.

[31] K. Vanommeslaeghe, E. Hatcher, C. Acharya, S. Kundu, S. Zhong, J. Shim, E. Darian, O. Guvench, P. Lopes, I. Vorobyov, A.D. Mackerell, Jr., CHARMM general force field: A force field for drug-like molecules compatible with the CHARMM all-atom additive biological force fields, J. Comput. Chem. 31(4) (2010) 671-90.

[32] J. Yoo, J. Wilson, A. Aksimentiev, Improved model of hydrated calcium ion for molecular dynamics simulations using classical biomolecular force fields, Biopolymers 105(10) (2016) 752-63.

[33] T.O. Wambo, L.Y. Chen, S.F. McHardy, A.T. Tsin, Molecular dynamics study of human carbonic anhydrase II in complex with Zn(2+) and acetazolamide on the basis of all-atom force field simulations, Biophys. Chem. 214-215 (2016) 54-60.

[34] H. Motulsky, A. Christopoulos, ProQuest (Firm), Fitting models to biological data using linear and nonlinear regression : a practical guide to curve fitting.

[35] M.J. Lew, J.A. Angus, Analysis of competitive agonist-antagonist interactions by nonlinear regression, Trends Pharmacol. Sci. 16(10) (1995) 328-37.

[36] O. Arunlakshana, H.O. Schild, Some quantitative uses of drug antagonists, Br. J. Pharmacol. Chemother. 14(1) (1959) 48-58.

[37] G.V. Born, J.B. Smith, Uptake, metabolism and release of (3H)-adrenaline by human platelets, Br. J. Pharmacol. 39(4) (1970) 765-78.

[38] O.A. Nedergaard, A. Vagne, J.A. Bevan, Effect of the chelating agents, EDTA, 2,2'-bipyridine, 8-hydroxyquinoline and pyrophosphoric acid, on norepinephrine uptake by rabbit aorta, J. Pharmacol. Exp. Ther. 163(1) (1968) 136-46.

[39] M. Stone, J.A. Angus, Developments of computer-based estimation of pA_2 values and associated analysis, J. Pharmacol. Exp. Ther. 207(3) (1978) 705-18.

[40] P.W. Abel, K.P. Minneman, Alpha-1 adrenergic receptor binding and contraction of rat caudal artery, J. Pharmacol. Exp. Ther. 239(3) (1986) 678-686.

[41] W.S. Colucci, T.A. Brock, M.A. Gimbrone, R.W. Alexander, Nonlinear relationship between α_1-adrenergic receptor occupancy and norepinephrine-stimulated calcium flux in cultured vascular smooth muscle cells, Mol. Pharmacol. 27(5) (1985) 517-524.

[42] T.P. Kenakin, Chapter 6 - Orthosteric drug antagonism, in: T.P. Kenakin (Ed.), A Pharmacology primer: techniques for more effective and strategic drug discovery, Academic Press, San Diego, 2014, pp. 119-154.

[43] C.J. Daly, C. Deighan, A. McGee, D. Mennie, Z. Ali, M. McBride, J.C. McGrath, A knockout approach indicates a minor vasoconstrictor role for vascular alpha1B-adrenoceptors in mouse, Physiol. Genomics 9(2) (2002) 85-91.

[44] C. Hague, M.A. Uberti, Z. Chen, R.A. Hall, K.P. Minneman, Cell Surface Expression of α_{1D}-Adrenergic Receptors Is Controlled by Heterodimerization with α_{1B}-Adrenergic Receptors, J. Biol. Chem. 279(15) (2004) 15541-15549.

[45] S. Ma, Y. Chen, A. Dai, W. Yin, J. Guo, D. Yang, F. Zhou, Y. Jiang, M.W. Wang, H.E. Xu, Structural mechanism of calcium-mediated hormone recognition and Gβ interaction by the human melanocortin-1 receptor, Cell Res. 31(10) (2021) 1061-1071.

[46] E. Tomat, E.M. Nolan, J. Jaworski, S.J. Lippard, Organelle-specific zinc detection using Zinpyr-labeled fusion proteins in live cells, J. Am. Chem. Soc. 130(47) (2008) 15776-15777.

[47] P.A. Adlard, R.A. Cherny, D.I. Finkelstein, E. Gautier, E. Robb, M. Cortes, I. Volitakis, X. Liu, J.P. Smith, K. Perez, K. Laughton, Q.-X. Li, S.A. Charman, J.A. Nicolazzo, S. Wilkins, K. Deleva, T. Lynch, G. Kok, C.W. Ritchie, R.E. Tanzi, R. Cappai, C.L. Masters, K.J. Barnham, A.I. Bush, Rapid restoration of cognition in Alzheimer's transgenic mice with 8-hydroxy quinoline analogs is associated with decreased interstitial Aβ, Neuron 59(1) (2008) 43-55.

[48] M.H. Park, S.J. Lee, H.R. Byun, Y. Kim, Y.J. Oh, J.Y. Koh, J.J. Hwang, Clioquinol induces autophagy in cultured astrocytes and neurons by acting as a zinc ionophore, Neurobiol. Dis. 42(3) (2011) 242-51.

[49] D.M.B. Boedtkjer, V.V. Matchkov, E. Boedtkjer, H. Nilsson, C. Aalkjaer, Vasomotion has chloride-dependency in rat mesenteric small arteries, Pflugers Arch. 457(2) (2008) 389.

[50] G. Swaminath, T.W. Lee, B. Kobilka, Identification of an allosteric binding site for Zn^{2+} on the β_2 adrenergic receptor, J. Biol. Chem. 278(1) (2003) 352-6.

[51] J. Alvarez-Collazo, C.M. Diaz-Garcia, A.I. Lopez-Medina, G. Vassort, J.L. Alvarez, Zinc modulation of basal and β-adrenergically stimulated L-type Ca^{2+} current in rat ventricular cardiomyocytes: consequences in cardiac diseases, Pflugers Arch. 464(5) (2012) 459-70.

[52] P.T. McKeny, T.A. Nessel, P.M. Zito, Antifungal Antibiotics, StatPearls [Internet], StatPearls Publishing, Treasure Island (FL), 2023 Jan.

[53] W.A. Pettinger, H.C. Mitchell, Side effects of vasodilator therapy, Hypertension 11(3 Pt 2) (1988) Ii34-6.

Table 1. Molecular dynamics simulations of clioquinol binding to the human α_1-adrenoceptor investigating cation-bridged interactions.

No	Ligand	Ligand Position	Counterion
S1	-	-	Na^+
S2	QAPB	Orthosteric	-
S3	Clioquinol	Orthosteric	Na^+
S4	Clioquinol	Outer vestibule	Na^+
S5	Clioquinol	Orthosteric	Ca^{2+}
S6	Clioquinol	Orthosteric	Zn^{2+}

QAPB - BODIPY-FL-prazosin

Table 2: The effects of clioquinol on the pEC_{50} and E_{max} of methoxamine (MeOx)-induced extracellular calcium-dependent contraction in rat isolated mesenteric arteries.

Treatment	pEC_{50}	E_{max} (% KPSS)	n
Controls			
1st curves (with MeOx 10 μM)	3.95 ± 0.06	118 ± 2	8
2nd curves, time control	3.89 ± 0.07	118 ± 4	4

2nd curves, vehicle control	3.93 ± 0.11	112 ± 7	4
Clioquinol			
Control 1st curve (with MeOx 10 µM)	3.92 ± 0.03	111 ± 4	13
+ Clioquinol 3 µM	3.73 ± 0.04**	107 ± 4	5
+ Clioquinol 10 µM	3.49 ± 0.05***	101 ± 6	5
+ Clioquinol 30 µM	N/A	2 ± 1***	4
Zn(DTSM)			
Control 1st curve (with MeOx 10 µM)	3.87 ± 0.04	111 ± 2	12
+ Zn(DTSM) 3 µM	3.57 ± 0.07**	114 ± 4	4
+ Zn(DTSM) 10 µM	3.20 ± 0.07***	41 ± 16****	5
+ Zn(DTSM) 30 µM	N/A	2 ± 1****	4

Responses were tested after arteries were washed with calcium-free PSS and stimulated with methoxamine (MeOx, 10 µM) and extracellular calcium reintroduced. E_{max}, the maximum contractile responses caused by calcium expressed as a % of the maximum KPSS reference contraction; pEC_{50}, $-\log_{10}EC_{50}$; Zn(DTSM), zinc(II) 3,4-hexanedione bis[N(4)-methylthiosemicarbazone. **p<0.01, ***p<0.001, ****p<0.0001 compared to the control 1st curve, 1-way ANOVA with Dunnett's post-test. Values are mean ± 1 SEM. N/A, not applicable; n, number of arteries isolated from separate rats.

Figure Legends

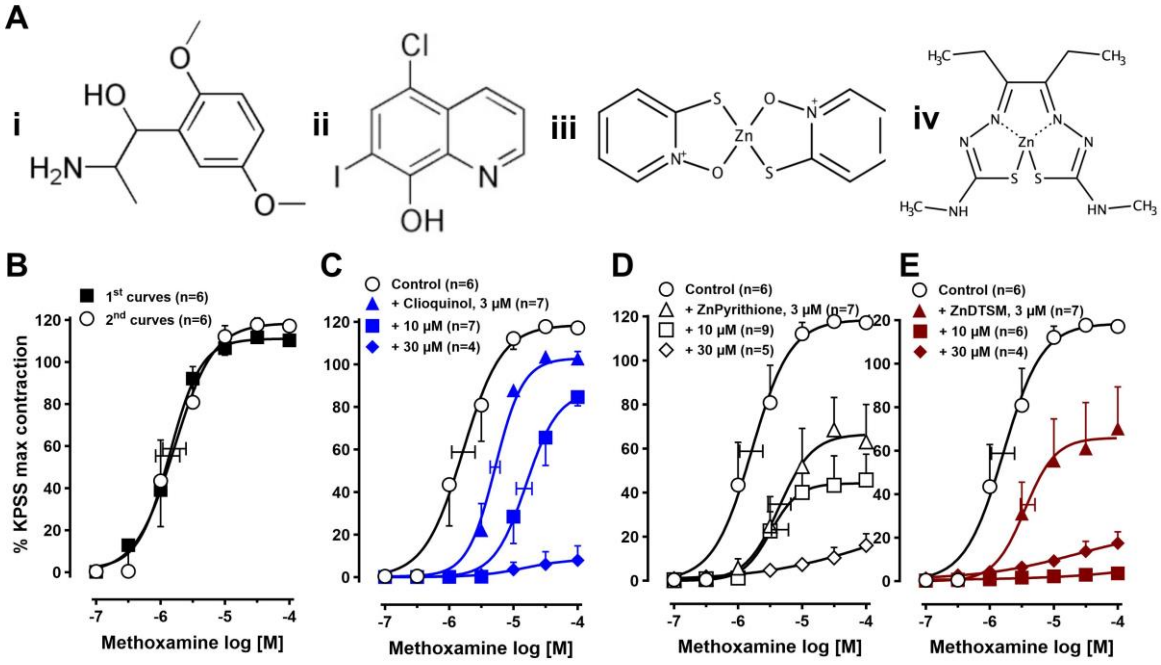

Figure 1: Effects of zinc ionophores on α_1-adrenoceptor-mediated contraction.

Chemical structures of methoxamine (**i**), clioquinol (**ii**), zinc pyrithione (**iii**) and Zn(DTSM) (**iv**). (**B**) Control methoxamine concentration response curves (1st curves) and repeated second curves in the same arteries that serve as the control. Effects of different concentrations of clioquinol (**C**), zinc pyrithione (**D**) and Zn(DTSM) (**E**) on the α_1-adrenoceptor agonist-mediated contraction. Responses are expressed as a % of the KPSS reference contraction. Vertical error bars are ± 1 SEM (those not shown are contained within the symbol) and horizontal error bars represent the average EC_{50} ± 1 SEM. n, number of arteries isolated from separate rats.

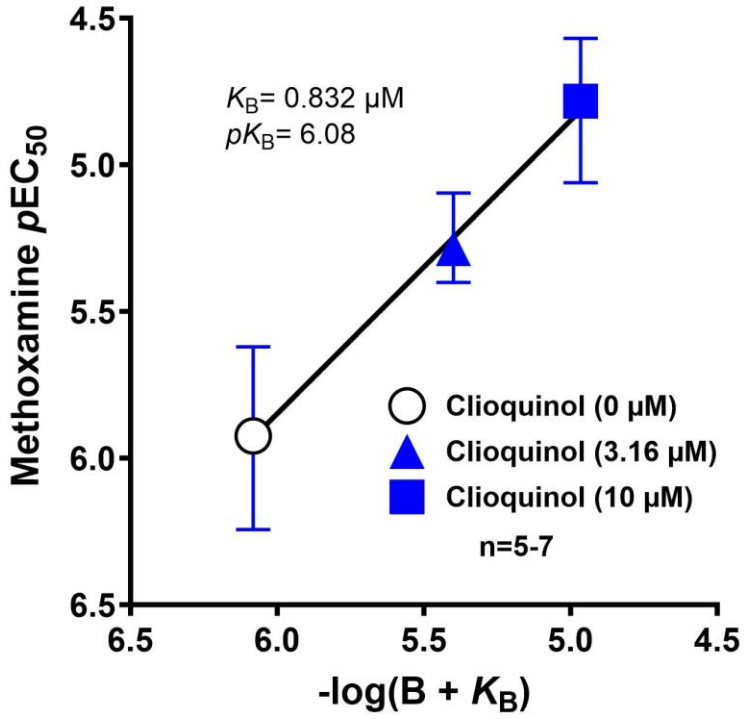

Figure 2: Clark plot display of the relationship between the pEC_{50} (-log M) of methoxamine and the antagonist, clioquinol, –log(B + K_B) concentration in rat mesenteric arteries.

The dissociation constant of clioquinol (K_B) by non-linear regression was calculated to be 0.832 µM (6.08 pK_B). The antagonist, clioquinol, concentration (B) was 0, 3.16 µM or 10 µM. Error bars are ± 2SEM of the difference between the agonist pEC_{50} values fitted for individual arteries in the presence of each concentration of antagonist, clioquinol (B), and the predicted fitted pEC_{50} value of agonist from the non-linear regression. n, number of arteries isolated from separate rats.

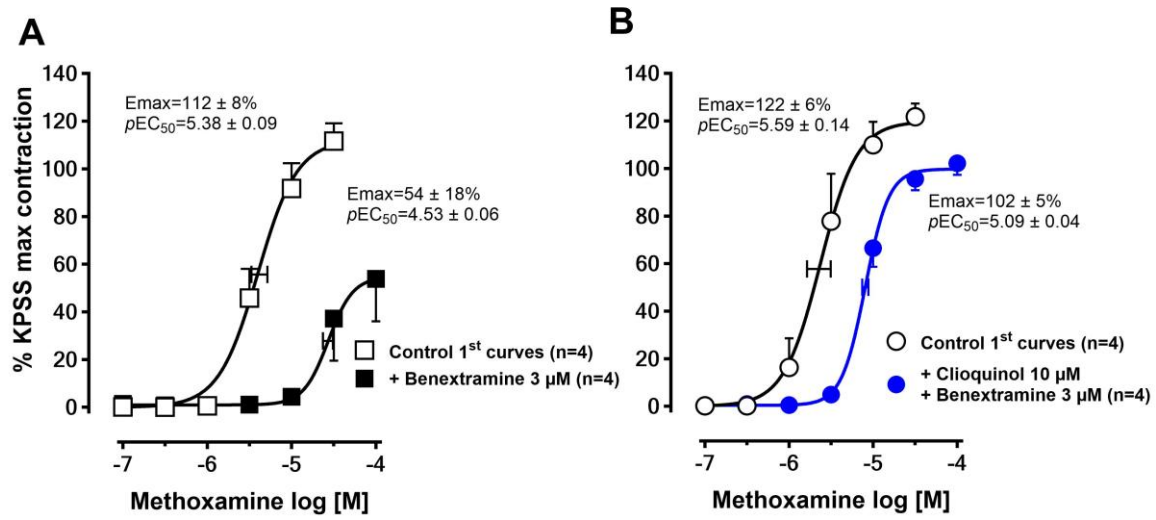

Figure 3: Clioquinol pre-treatment protects irreversible blockade of α_1-adrenoceptor-mediated contraction by benextramine.

Methoxamine concentration-contraction curves were first completed in rat isolated small mesenteric arteries in the absence of any treatment (control 1st curves). Then subsets of these arteries were incubated with either incubation with vehicle (open black squares and circles) as control for 30 min followed by 3 µM benextramine for 5 min (**A**) or incubation with 10 µM clioquinol (blue circles) for 30 min to bind and protect α_1-adrenoceptors followed by 3 µM benextramine for 5 min (**B**). Responses are expressed as a % of the KPSS reference contraction. Vertical error bars are ± 1 SEM (those not shown are contained within the symbol) and horizontal error bars represent the average EC_{50} ± 1 SEM. n, number of arteries isolated from separate rats.

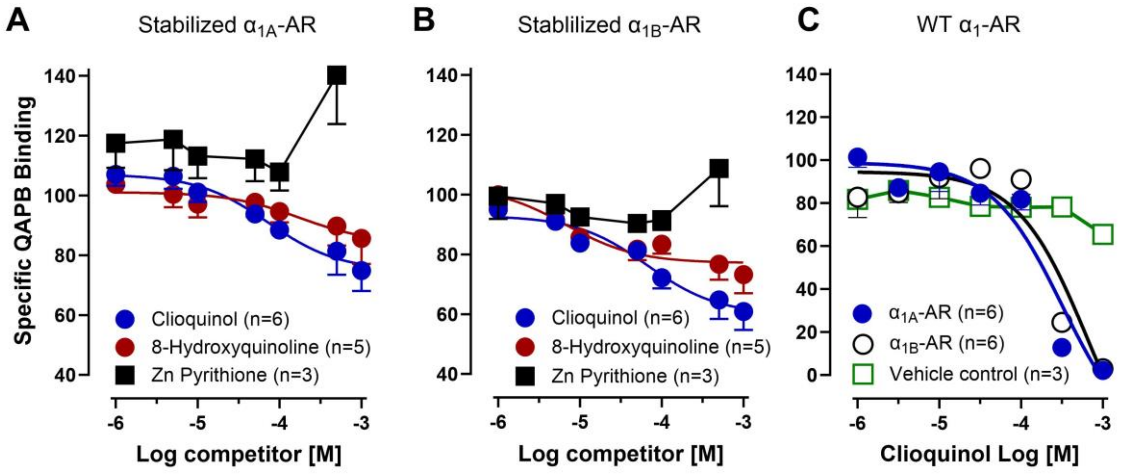

Figure 4. Competitive binding profile in stabilized and wild-type human α_{1A}- and α_{1B}-adrenoceptors expressed in COS-7 cells. Increasing concentrations of non-fluorescent clioquinol, 8-hydroxyquinoline or zinc pyrithione were used to compete for binding with solubilized and stable α_{1A}- (**A**) or α_{1B}-adrenoceptors (**B**) with the selective and fluorescently labelled antagonist BODIPY-FL-prazosin (QAPB, 6.25 nM). (**C**) The equilibrium binding of QAPB was inhibited by clioquinol in COS-7 cells expressing wild type (WT) human α_{1A}- or α_{1B}-adrenoceptors. All assays were performed using 6.25 nM QAPB for 1 h at 20°C. Data points represent the mean ± SEM of 3-6 independent experiments performed in duplicate.

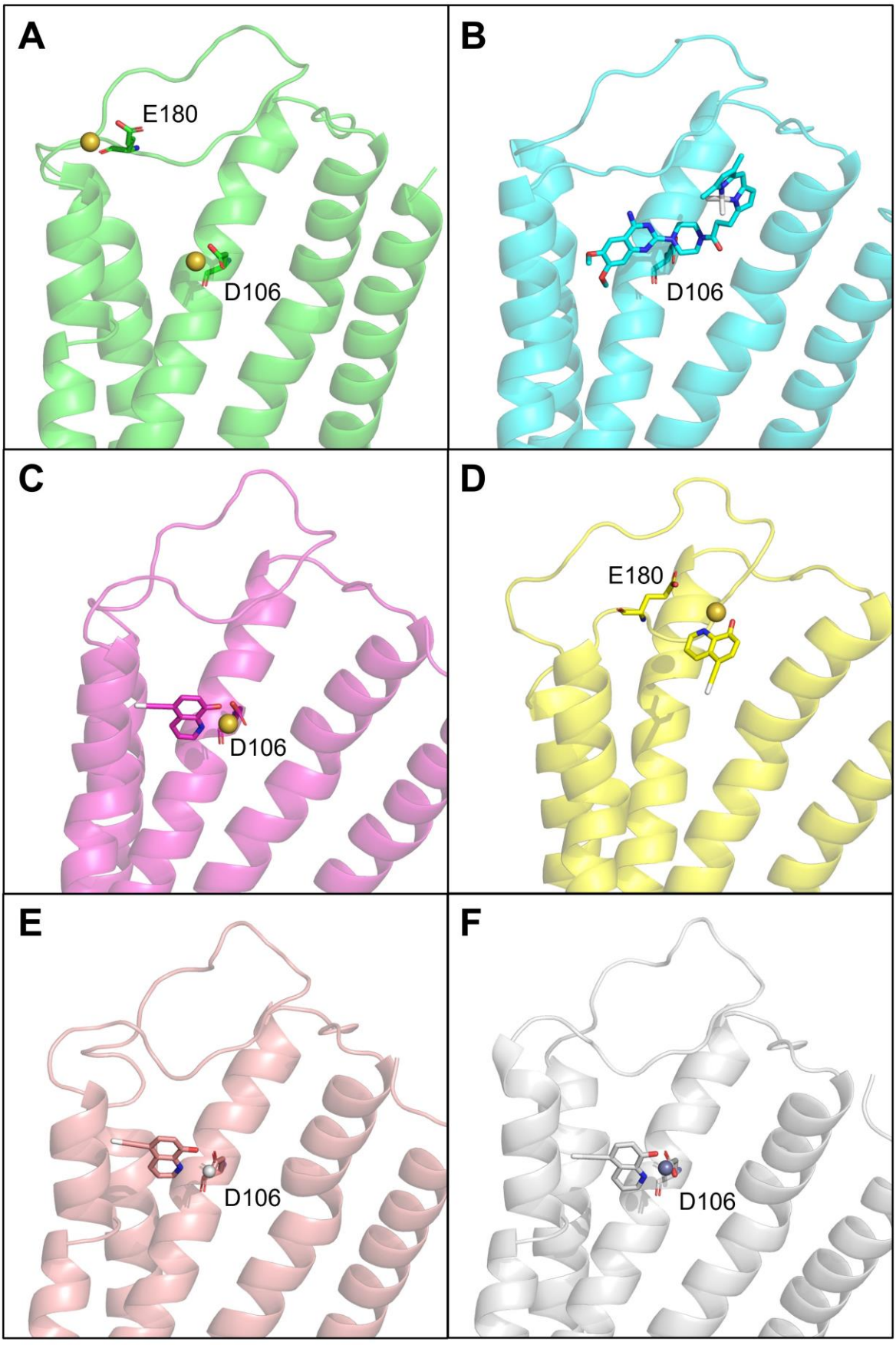
A
E180
D106
B
D106
C
D106
D
E180
E
D106
F
D106

Figure 5. Molecular dynamics simulations of clioquinol binding to the human α_{1A}-adrenoceptor. (**A**) Two sodium binding sites on the α_{1A}-adrenoceptor in simulation S1, one near Glu180 and another near Asp106. (**B**) Bound conformation of QAPB to α_{1A}-adrenoceptor. (**C**) Stable clioquinol in orthosteric bound pose from simulation S3. (**D**) Initial docked pose of unstable outer vestibule binding of clioquinol. (**E**) Simulation S5 of clioquinol in the orthosteric binding site with Ca^{2+} cation bridge. (**F**) Simulation S6 of clioquinol in the orthosteric binding site with Zn^{2+} cation bridge.

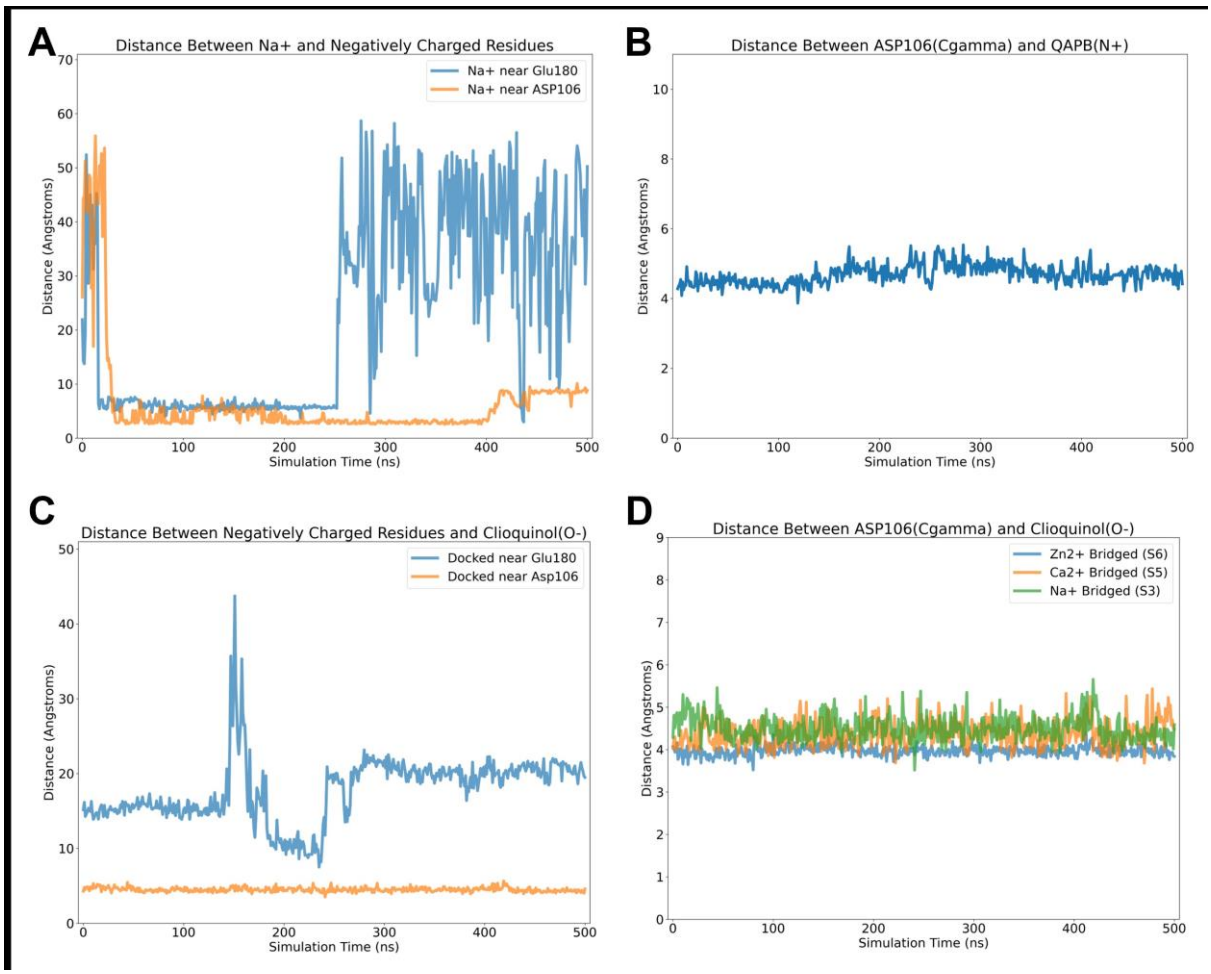

Figure 6. Distance measurements over molecular dynamics simulation time.

(**A**) Simulation S1 of the apo state simulation showing distances between ions and residues Glu 180 and Asp 106. Ions bind to these residues for > 200 ns. (**B**) Simulation S2 of bound QAPB simulation showing that the ligand remains stable for the full simulation. (**C**) Orthosteric bound

clioquinol S3 is more stable than outer pocket bound S4. (**D**) Substitution of sodium S3 with divalent cations S5&6 in orthosteric site does not affect binding.

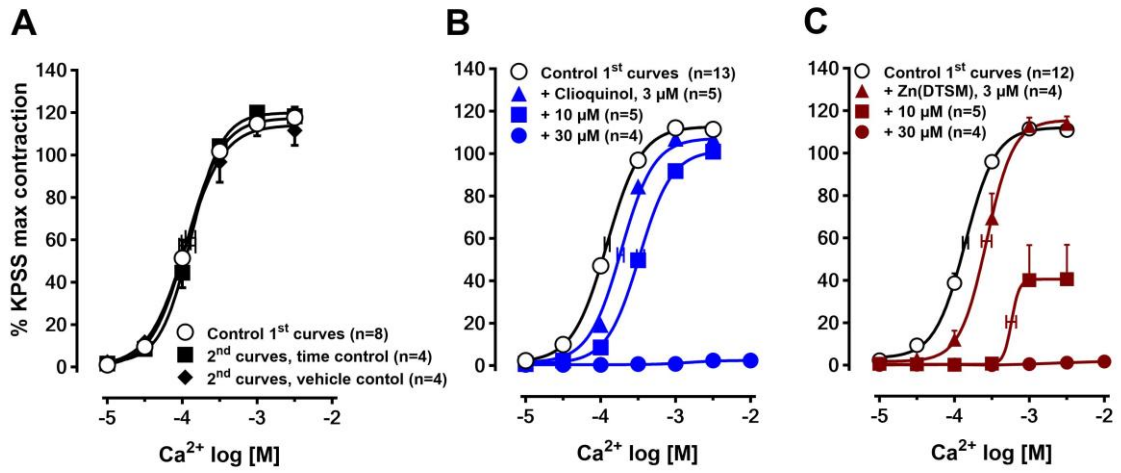

Figure 7: Contraction of isolated small mesenteric arteries induced by α_1-adrenoceptor-dependent influx of Ca^{2+} without or with clioquinol.

(**A**) Control calcium curves for time and vehicle (maximum volume of DMSO used at the highest concentration of clioquinol). (**B**) The effects of different concentrations of clioquinol or (**C**) ZnDTSM on the calcium-dependent contraction induced by the α_1-adrenoceptor agonist methoxamine. The rat isolated mesenteric arteries were first washed with calcium-free PSS followed by stimulation with methoxamine (10 µM) and contraction curve to an increasing concentration of calcium (control 1st curves), wash, 15 min incubation with a single concentration of the treatment and repetition of the calcium curve in the presence of methoxamine (2nd curve). The controls in each figure are pooled 1st curves for all the treatment groups in the specific figure. Responses are expressed as a % of the KPSS reference contraction. Vertical error bars are ± 1 SEM (those not shown are contained within the symbol) and horizontal error bars represent the average EC_{50} ± 1 SEM. n, number of arteries isolated from separate rats.

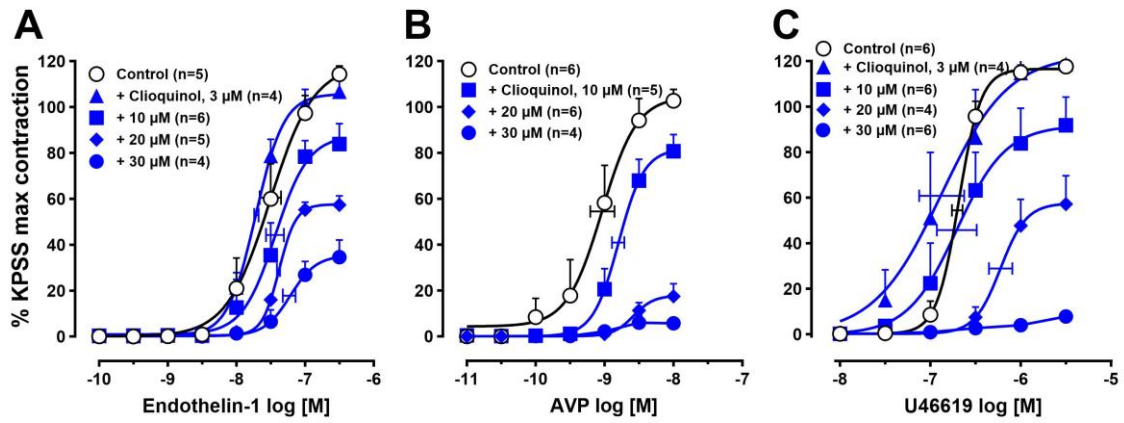

Figure 8: Clioquinol non-competitively inhibits contractions induce by endothelin-1, arginine vasopressin (AVP) or U46619 in isolated rat mesenteric arteries.

Concentration-dependent contractions induced by endothelin-1 (**A**), AVP (**B**) or the thromboxane A_2-mimetic U46619 (**C**) in rat isolated small mesenteric arteries were non-competitively antagonized by pre-treatment (30 min) with different concentrations of clioquinol. Responses are expressed as a % of the KPSS reference contraction. Vertical error bars are ± 1 SEM (those not shown are contained within the symbol) and horizontal error bars represent the average EC_{50} ± 1 SEM. n, number of arteries isolated from separate rats.